

# Hyperuniformity in the Frustrated Vicsek-Kuramoto Model

Yichen Lu

November 24, 2025

## Contents

<a href="#">1 The Model</a>	<a href="#">1</a>
<a href="#">2 Simulation Results</a>	<a href="#">2</a>

## 1 The Model

Particles are described by position  $\mathbf{r}_i = (x_i, y_i)$  and phase angle  $\theta_i$ , evolving as:

$$\dot{\mathbf{r}}_i = v \mathbf{p}(\theta_i) , \quad (1a)$$

$$\dot{\theta}_i = \frac{K}{|A_i|} \sum_{j \in A_i} [\sin(\theta_j - \theta_i + \alpha) - \sin \alpha] , \quad (1b)$$

where  $A_i(t) = \{j : |\mathbf{r}_i(t) - \mathbf{r}_j(t)| \leq d_0\}$  is the set of neighbors within coupling radius  $d_0$ ,  $K (\geq 0)$  is coupling strength, and  $\alpha$  is frustration. The term  $-\sin \alpha$  ensures synchronization ( $\theta_j = \theta_i$ ) remains an equilibrium [8]. This model generalizes alignments [3, 6, 7, 9, 10], anti-alignments [1, 2], and chimera states [4, 5]. It reduces to normal Vicsek-Kuramoto for  $\alpha = 0$  and anti-aligning interactions for  $\alpha = \pi$ .

## 2 Simulation Results

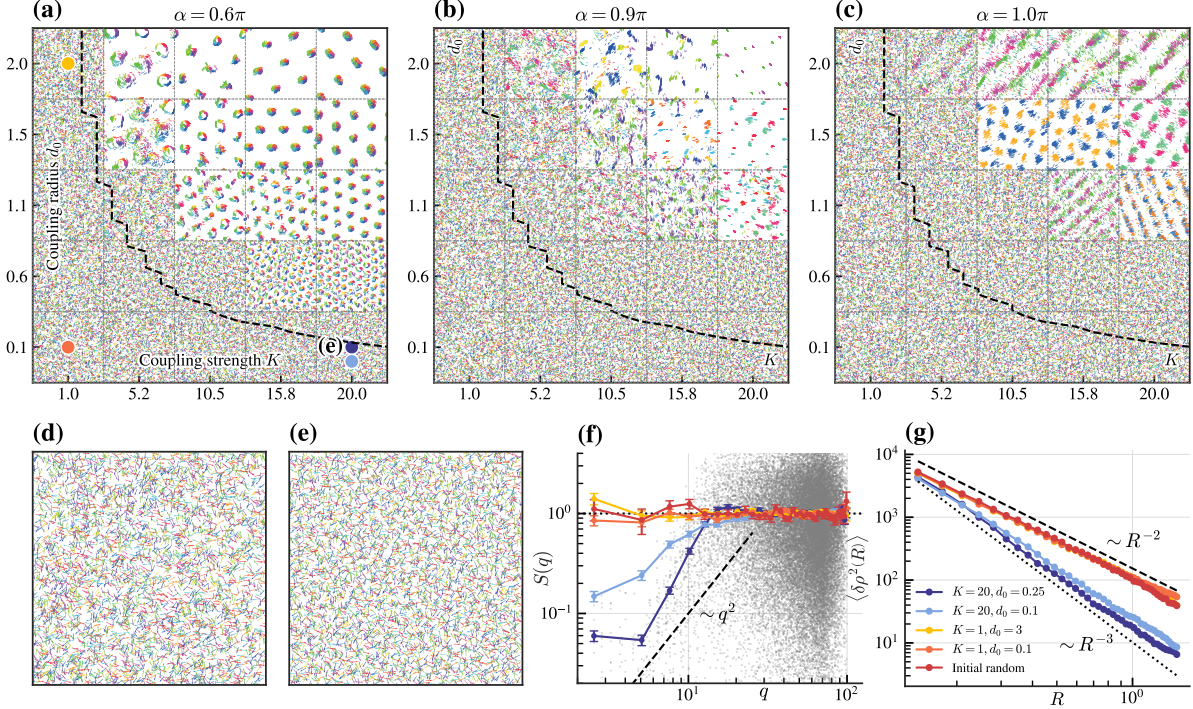


Figure 1: (a)-(c) Snapshots of  $(K, d_0)$  phase diagram under different frustration  $\alpha$  for  $L = 7, N = 2000$  and  $v = 3$ . The boundaries between dominant and recessive lattice states, are indicated with black dashed lines. (d), (e) Snapshots comparing random uniform initial conditions (d) and the resulting hyperuniform final state (e) for  $K = 20, d_0 = 0.25, \alpha = 0.6\pi$  and  $N = 5000$  (large population for better showcase). Hyperuniformity of the recessive lattice states is characterized by the structure factor  $S(q)$  in (f) and the density variance  $\langle \delta\rho^2(R) \rangle$  in (g). Black dashed lines indicate the scaling behaviors  $S(q) \sim q^{-2}$  and  $\langle \delta\rho^2(R) \rangle \sim R^{-2,-3}$ , respectively. In (f), gray dots represent the sample of  $S(\mathbf{q}_n)$  for periodic boundary conditions allowed wavevectors  $\mathbf{q}_n = (2\pi n_1/L, 2\pi n_2/L)$  with  $\mathbf{n} \in (\mathbb{Z}^*)^2$  at  $K = 20, d_0 = 0.25$ , and the point-fold curves with error bars show the binned average and standard deviation of their respective  $S(\mathbf{q}_n)$ . Solid dots and text label in (a) mark the location in  $(K, d_0)$  phase diagram corresponding to the parameters analyzed in (e)-(g).

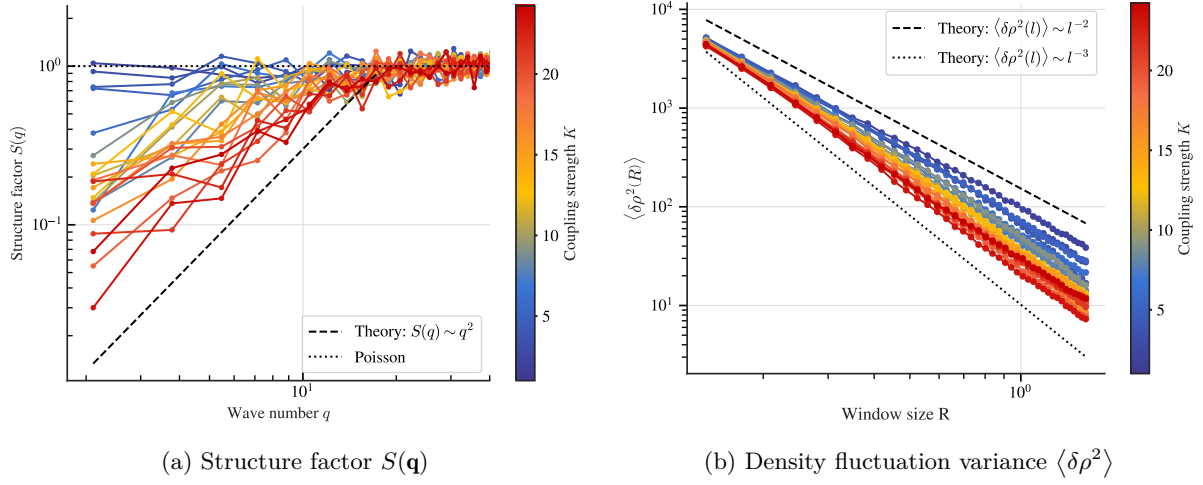


Figure 2: (a) Structure factor  $S(\mathbf{q})$  for varying coupling strength  $K$  for  $\alpha = 0.6\pi, d_0 = 0.1$ . (b) Density fluctuation variance  $\langle \delta \rho^2 \rangle$  as a function of mean density  $\langle \rho \rangle$  for different  $K$  values.

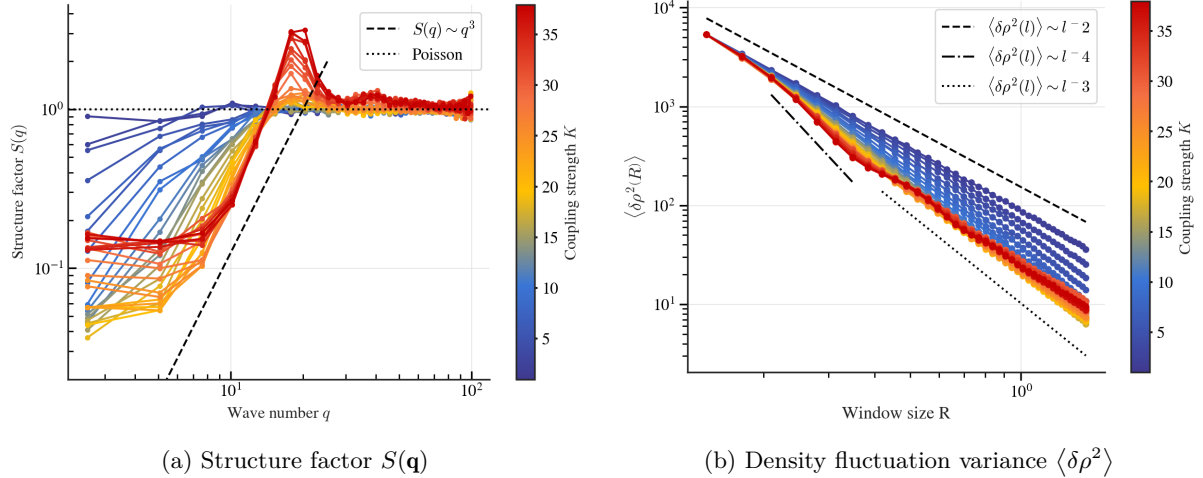


Figure 3: (a) Structure factor  $S(\mathbf{q})$  for varying coupling strength  $K$  for  $\alpha = 0.6\pi, d_0 = 0.25$ . (b) Density fluctuation variance  $\langle \delta \rho^2 \rangle$  as a function of mean density  $\langle \rho \rangle$  for different  $K$  values.

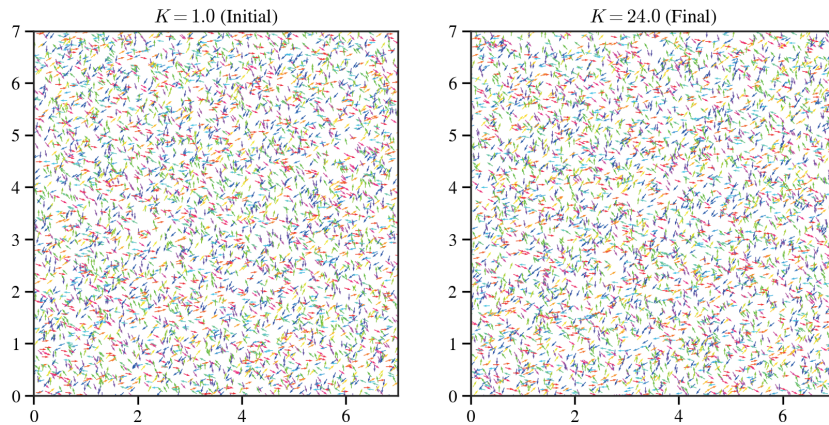


Figure 4: Forward snapshots.

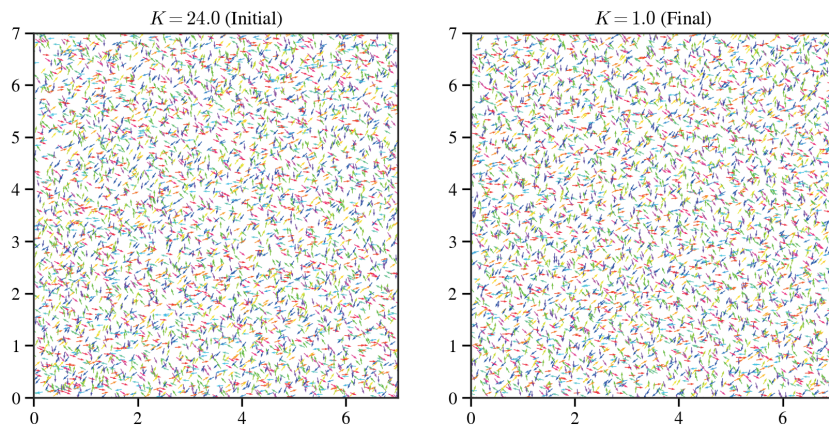


Figure 5: Backward snapshots.

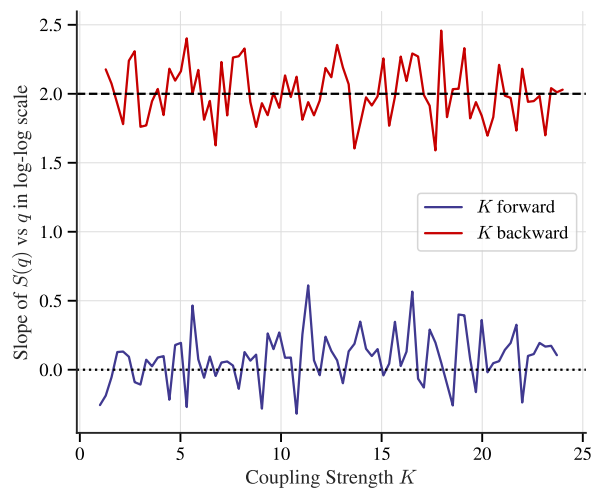


Figure 6: The slope of  $S(q)$  in the small- $q$  regime as a function of coupling strength  $K$  at fixed frustration  $\alpha = 0.6\pi$ .

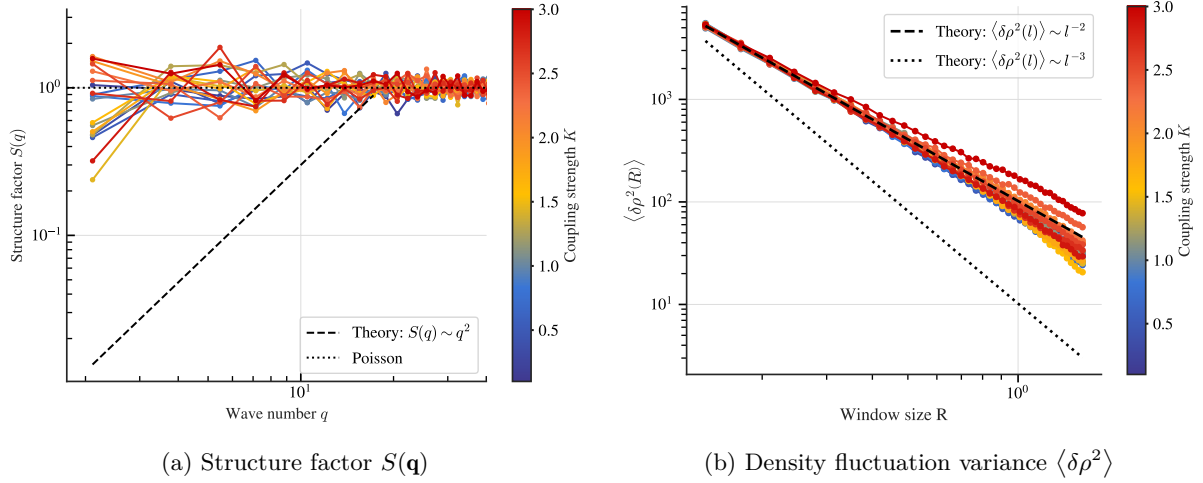


Figure 7: (a) Structure factor  $S(\mathbf{q})$  for varying coupling radius  $d_0$  at fixed frustration  $\alpha = 0.6\pi$ . (b) Density fluctuation variance  $\langle \delta\rho^2 \rangle$  as a function of mean density  $\langle \rho \rangle$  for different  $K$  values.

## References

- [1] Daniel Escaff. Anti-aligning interaction between active particles induces a finite wavelength instability: The dancing hexagons. *Phys. Rev. E*, 109:024602, Feb 2024.
- [2] Daniel Escaff. Self-organization of anti-aligning active particles: Waving pattern formation and chaos. *Phys. Rev. E*, 110:024603, Aug 2024.
- [3] Daniel Escaff and Rafael Delpiano. Flocking transition within the framework of kuramoto paradigm for synchronization: Clustering and the role of the range of interaction. *Chaos: An Interdisciplinary Journal of Nonlinear Science*, 30(8):083137, 08 2020.
- [4] Nikita Kruk, José A. Carrillo, and Heinz Koepll. Traveling bands, clouds, and vortices of chiral active matter. *Phys. Rev. E*, 102:022604, Aug 2020.
- [5] Nikita Kruk, Yuri Maistrenko, and Heinz Koepll. Self-propelled chimeras. *Phys. Rev. E*, 98:032219, Sep 2018.
- [6] D. Levis, I. Pagonabarraga, and B. Liebchen. Activity induced synchronization: Mutual flocking and chiral self-sorting. *Phys. Rev. Res.*, 1:023026, Sep 2019.
- [7] Benno Liebchen and Demian Levis. Collective behavior of chiral active matter: Pattern formation and enhanced flocking. *Phys. Rev. Lett.*, 119:058002, Aug 2017.
- [8] Hidetsugu Sakaguchi, Shigeru Shinomoto, and Yoshiki Kuramoto. Mutual entrainment in oscillator lattices with nonvariational type interaction. *Progress of Theoretical Physics*, 79(5):1069–1079, 05 1988.
- [9] Bruno Ventejou, Hugues Chaté, Raul Montagne, and Xia-qing Shi. Susceptibility of orientationally ordered active matter to chirality disorder. *Phys. Rev. Lett.*, 127:238001, Nov 2021.
- [10] Yujia Wang, Bruno Ventéjou, Hugues Chaté, and Xia-qing Shi. Condensation and synchronization in aligning chiral active matter. *Phys. Rev. Lett.*, 133:258302, Dec 2024.